JGR Earth Surface

RESEARCH ARTICLE
10.1029/2018JF004953

Incipient Tidal Bar and Sill Formation

J. R. F. W. Leuven[1] and M. G. Kleinhans[1]

[1] Faculty of Geosciences, Utrecht University, Utrecht, The Netherlands

Abstract Estuaries and rivers show dynamic patterns of bars and channels. Mutually evasive ebb- and flood-dominated tidal channels, that is, parallel tidal channels with net sediment transport in opposing directions, give tidal bars their characteristic shape. Here, we study incipient tidal bars with laboratory scale experiments in a periodically tilting flume. Bar patterns evolved from an initial straight channel in an erodible sand bed. Analysis of time-lapse imagery and bathymetry shows that alternate bars form within 300 tidal cycles. The bars become discrete, recognizable elements after an initial phase characterized by a rhomboid pattern (short and narrow ridges oblique to the channel). Tidal bars show similarities and contrasts with fluvial bars. In general, morphological shapes are similar, including the presence of alternate bars, midchannel bars, and point bars. Sills are superimposed on incipient tidal bars. Sills are narrow and straight and form by flow divergence and thus sediment convergence between alternate bars. This contrasts with rivers, where sills are remnants of alternate bars. Alternate tidal bars grow further by amalgamation of two opposing U-shaped lobate bars. The dimensions of incipient tidal bars emerge in the first 500 cycles, after which their length and position determine a large-scale quasiperiodic variation in the estuary width. The results imply that sills are initiated with the onset of tidal bar formation in straight channels and trigger formation of mutually evasive ebb- and flood-dominated channels, thus explaining their ubiquitous occurrence in tidal systems.

Key Points:
- A sill that forms and persists between incipient alternate bars is unique for tidal systems
- A deep, poorly connected channel flanks alternate tidal bars, from where flow divergence on both ends causes sediment deposition in the sill
- The sills trigger formation of mutually evasive channels, explaining their stable presence in nature even in absence of topographic forcing

Supporting Information:
- Supporting Information S1
- Movie S1

Correspondence to:
J. R.F.W. Leuven,
j.r.f.w.leuven@uu.nl

Citation:
Leuven, J. R. F. W., & Kleinhans, M. G. (2019). Incipient tidal bar and sill formation. *Journal of Geophysical Research: Earth Surface*, *124*, 1762–1781. https://doi.org/10.1029/2018JF004953

Received 14 NOV 2018
Accepted 22 MAY 2019
Accepted article online 2 JUN 2019
Published online 10 JUL 2019

1. Introduction

Estuaries are tidal systems that occur where rivers flow into the sea. Many estuaries were formed in valleys that drowned under fast rising sea level during the early to middle Holocene (e.g., de Haas et al., 2017; Hijma & Cohen, 2011; van der Spek & Beets, 1992) and were subsequently infilled with sediment from the river and from the sea when sea level rise decelerated. Dynamic patterns of bars, also called shoals, and channels evolved as a result of the bidirectional tidal currents (Figure 1).

Perhaps the most typical and unique feature of channel patterns in tidal basins and estuaries is the presence of the mutually evasive ebb- and flood-dominated tidal channels (Figure 1), which are predominantly used during either the ebb or the flood phase (Dalrymple & Choi, 2007; Fenies & Faugères, 1998; Hibma et al., 2003; Kleinhans, Scheltinga, et al., 2015; van Veen, 1950). This process results in linear bars when the channels simply evade each other laterally but can also form U-shaped bars when one of the channels bifurcates around an opposing channel that is met head-on (Leuven et al., 2016). Van Veen already observed and described these striking elements in the 1950s and associated them to meandering of the main channel, which suggests that they are caused by topographic forcing.

It has been debated for quite a long time whether tides can shape forced and free bars as in river systems (Bridges & Leeder, 1976; Whiting & Dietrich, 1993). Only recently, stability theory showed that bars in straight and meandering tidal channels form from a similar instability mechanism as in rivers (Solari et al., 2002). Also, data showed that tidal meanders resemble river meanders in dimensions and behavior (Finotello et al., 2018; Lagasse et al., 2004; Leuven et al., 2018a). Free nonmigratory bars form due to an instability of the bed above threshold values for width-to-depth ratio and mean Shields sediment mobility (Schramkowski et al., 2002; Seminara & Tubino, 2001), while similar instability mechanisms in meandering channels lead to point bar-pool patterns (Solari et al., 2002). Overtides that cause ebb or flood asymmetry lead to net migration of tidal bars (Garotta et al., 2006). The fact that instability mechanisms for tidal bar formation are similar to rivers leads to the expectation that morphology and development of fluvial and tidal bars are similar.

Incipient bar formation and meandering has been thoroughly studied for rivers in scale experiments (Ashmore, 1982; Eaton et al., 2006; Frascati & Lanzoni, 2013; Fujita & Muramoto, 1985; Ikeda, 1973;

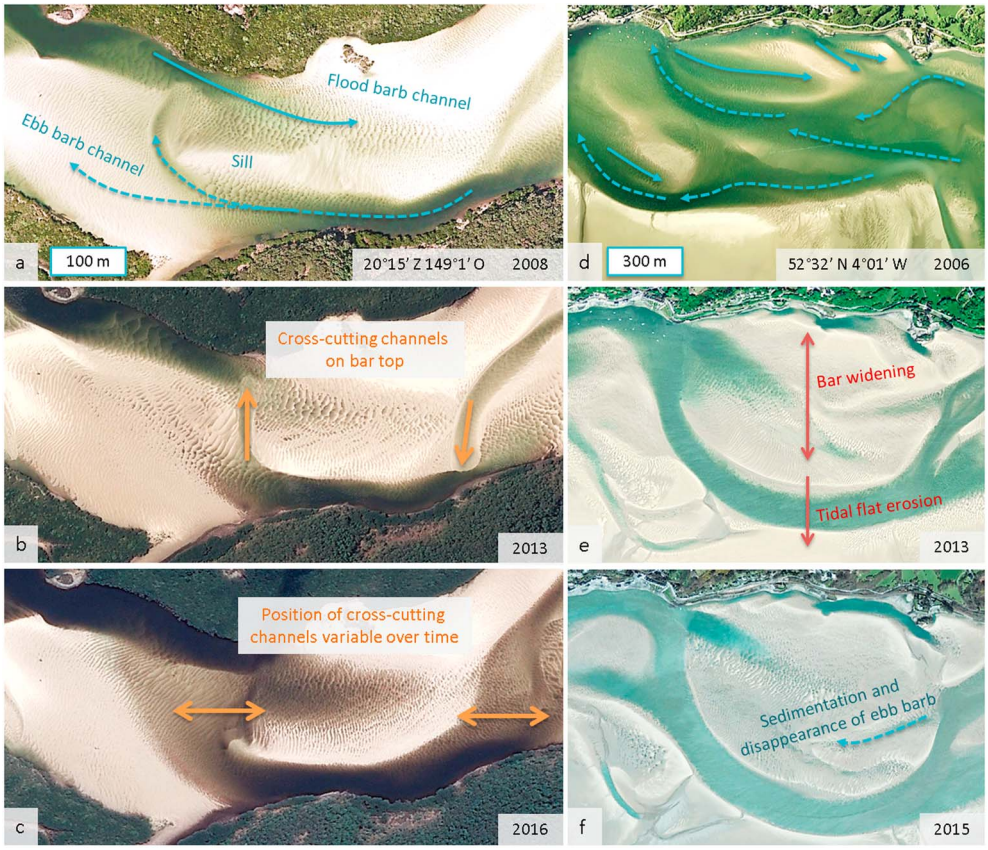

Figure 1. Dynamics of bars and mutually evasive ebb- and flood-dominated channels at (a–c) Whitehaven Beach (Australia) and in (d–f) the Dovey Estuary. (a, d) Tidal flow forms ebb and flood barbs, isolating a narrow and elongated sill between the mutually evasive channels. (b, c) Water level gradients cause cross-cutting channels on top of the sill. (e, f) Channels and bars are very dynamic over time, causing tidal flat and salt marsh erosion and formation.

van de Lageweg et al., 2014; Leopold & Wolman, 1957; Visconti et al., 2010), numerical models (Schuurman et al., 2013), theoretical models (Repetto et al., 2002; Seminara & Tubino, 1989; Struiksma et al., 1985), and natural systems (Ashworth et al., 2000; Cant & Walker, 1978; Lewin, 1976; Sambrook Smith et al., 2006). In summary (review by Kleinhans, 2010), the channel width and depth are determined by the balance between bank erosion and floodplain formation. The width and width-to-depth ratio subsequently determine whether the bar pattern becomes meandering or braided. A combination of bank retreat and bar and floodplain formation (Eke, 2014; Parker et al., 2011; van de Lageweg et al., 2014) causes migration of bars in meandering channels, which implies that increased resistance in floodplain material reduces channel migration. Wider channels form midchannel bars that bifurcate the flow. Such bifurcations are inherently unstable in the majority of rivers on Earth, which is also associated to the process of active braiding. This leads to asymmetrical bifurcations such that one channel becomes the main path for flow and sediment (Bolla Pittaluga et al., 2015; Kleinhans et al., 2013). However, in the tidal environment, bifurcations of mutually evasive ebb- and flood-dominated tidal channels show opposed asymmetries by deflecting the flow asymmetrically into opposite channels of similar size during the ebb and the flood phase. This raises the question what causes this, and whether, in contrast to bifurcations in rivers, their configuration might be stable over time.

Tidal channels appear somewhat discontinuous at the bifurcations because of a persistent shoal, or sill. Sills are smaller-scale morphological elements that are enclosed by ebb- and flood-dominated channels (Robinson, 1960; Tank, 1996; van Veen, 1950), unique to tidal systems. They are observed at transitions between successive bends, which are the channel thalweg inflection points (Figure 1a). Such topographic forcing of flow in two opposing channels causes the main flow momentum to cross the channel centreline in different locations for ebb and flood flow (Ahnert, 1960; van Veen, 1950). This, in turn, leads to the formation of a shoal in the thalweg inflection zone with opposed net sediment transport directions in the parallel

channels around it (van Veen, 1950). While sills resemble tidal bars in their elongated shape and dimensions, with lengths in the order of magnitude of the estuary width, they are smaller and much lower in height and commonly remain submerged over almost the entire tidal cycle. As such, the sills appear superimposed on the dominant pattern of bars and channels. When sills are located within the main navigable channel, regular dredging is typically required in order to maintain and secure shipping fairways to inland harbors (Sistermans & Nieuwenhuis, 2004; Verbeek et al., 1999).

Sills are not predicted by theory but did emerge in numerical models. In contrast to river systems, only a few numerical models (e.g., Hibma et al., 2003; van der Wegen & Roelvink, 2008) and theories (Garotta et al., 2006; Schramkowski et al., 2002; Seminara & Tubino, 2001; Solari et al., 2002) are available for bar initiation in tidal systems, and the presence of sills is only observed but not explained. Stability theories for both rivers and tidal systems predict that braiding index (BI), that is, the number of channels and bars in cross section, increases with channel width (Crosato & Mosselman, 2009; Schramkowski et al., 2002; Seminara & Tubino, 2001; Struiksma et al., 1985). However, in tidal systems the dominant bar length increases with the amplitude of tidal flow velocity, while river bars are less sensitive to flow velocity and mainly determined by channel width-to-depth ratio (Leuven et al., 2016). Numerical modeling showed that initial tidal bar length depends on both width and tidal flow velocity (Hibma et al., 2004). Moreover, initially straight tidal channels connected to form a weakly meandering channel with flood "barbs" (BI = 1.5) within century timescales (Hibma et al., 2003) as qualitatively described by van Veen (1950). Here, barb channels are dead-ended in either the ebb or the flood direction. Here we aim to link the formation of barb channels with the persistence of sills. We describe and explain the process of incipient tidal bar formation and mutually evasiveness of tidal channels. To this end, we conducted experiments in a tilting flume and monitored the initial evolution of bars and channels with high temporal resolution, that is, measurements every 100 tidal cycles.

Below, we will first describe the experimental setup and procedure for data collection. Subsequently, the process of incipient channel and bar formation is qualitatively and quantitatively described. In the discussion, incipient bar formation in tidal systems is explained and compared with other studies on tidal bars and the similarities with their fluvial counterparts are assessed.

2. Methods and Materials

Experiments in a tilting flume (20 m by 3 m), called the Metronome, recently proved useful to study the long-term evolution of bar patterns in estuaries (Braat et al., 2019; Leuven et al., 2018b). Tilting the entire flume creates sufficient sediment mobility in both the ebb and the flood direction, which is required to generate dynamic tidal morphology. Moreover, this setup for the first time allows the experimental recreation of a short reach within an estuary, allowing detailed study of bar formation in reversing flow. For a more detailed description of the design and hydrodynamics of the Metronome, see Kleinhans, van der Vegt, et al. (2017).

2.1. Experimental Setup and Procedure

In this study, we performed experiments with an initially straight channel with two open boundaries (Figure 2), recreating a reach within an estuary or a double-head tidal channel. After pilot experiments, a total of two experimental conditions were selected for monitoring (Table 1). The settings were selected based on a larger set of approximately 23 pilots and 20 well-monitored experiments that also attest to the repeatability of pattern and planform characteristics. Previous experiments with an initially converging channel provided insights on bar pattern formation (Braat et al., 2019; Leuven et al., 2018b), showing that both the bar width and BI depends on the position along the estuary. This means that it is not straightforward to describe the formation of incipient tidal bars in general. For this reason, the experimental setup was here modified to an initially straight channel with open boundaries on both ends of the channel, aimed at creating symmetrical reversing flow, which approximates the condition known in linear stability theory as rigid lid.

The Metronome floor was covered with a layer of 0.07-m erodible sand bed, in which an initial channel was carved. The sediment mixture (supporting information Figure S1) consisted of coarse sand (D50 = 0.52 mm, $\rho_s = 2,650$ kg/m^{-3}) characterized by a grain size distribution with a coarse right tail, which allowed for sufficient sediment mobility while minimizing the formation of scour holes (Kleinhans, Leuven, et al., 2017). The initial channel width was either 0.2 or 0.6 m (Table 1) and the sediment bed was approximately 16 m long and 3.0 m wide (Figure 2b).

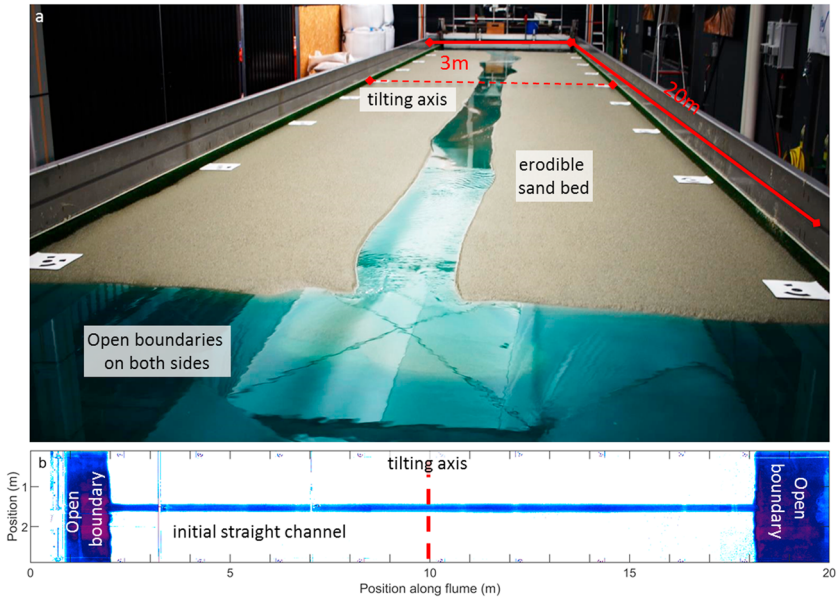

Figure 2. Experimental setup. (a) The Metronome, a tilting flume of 20 m long by 3 m wide. (b) Overhead image of the experimental setup for the experiment with a narrow channel (Exp. 017). An initial straight channel (0.2 m wide) with open boundaries on both sides. Blueness indicates depth except in the first meter where the gantry is located.

The seaward boundaries of the flume were open and connected by pumps to a large water reservoir. Water could freely flow out of the flume over a weir, which maintained a constant head at the sea. We compensated water depth in the sea for the tilting of the flume by periodically ($T = 40$ s) moving the weir up and down. This resulted in a constant water level at the boundary between the sediment bed and the sea. The water level was set to 0.065 m above the flume floor. Brilliant Blue FCF colorant was used to dye the water, allowing for the visualization of bar and channel morphology from overhead images.

Tidal currents were produced by flume tilting driven by four accurate actuators moving sinusoidally with a period of 40 s and a maximum tilting gradient of 0.008 m/m. The maximum tilting amplitude at the end basins of the flume was 75 mm. Tilting was such that sediment mobility was well above the threshold for motion and flow was turbulent and subcritical. We will evaluate these variables in the results section (Figure 10).

Multiple authors have described experimental scaling of bar and channel patterns (e.g., Kleinhans, Braudrick, et al., 2015; Lentsch et al., 2018; Tambroni et al., 2017). These studies showed that the most important scaling requirement is keeping sediment mobile during both the ebb and the flood phase, which is the case in our experiments (see Kleinhans, Scheltinga, et al. 2017, for Metronome scaling). Reducing the length or volume scale by, for example, a factor of 1,000 also results in a reduction of the timescale by the same order of magnitude. While we found in past experiments that the morphological changes were larger than expected from this scale (Kleinhans, Braudrick, et al., 2015), this is not deemed a problem because similar acceleration of morphological change in numerical models, for example, the Morfac approach (Ranasinghe et al., 2011; Roelvink, 2006), showed limited effects on the overall final morphology. Likewise, previous

Table 1
Experimental Settings

Nr	Type	a (mm)	T (s)	W (cm)	Bed level (mm)	MSL (mm)	t (cycles)
017	narrow	75	40	20	70	65	6,000
014	wide	75	40	60	70	65	3,100

Note. a is maximum tilting amplitude at the end basins of the flume, T is tilting period, W is initial channel width, bed level is the height of the plane sediment bed above the flume floor, MSL is the mean sea level above the flume floor, and t is the duration of the experiment.

experiments on tidal systems showed that bar proportions in three dimensions compare well with natural systems (Leuven et al., 2018b).

2.2. Data Collection and Data Processing

During the experiments, the following data were collected: overhead time-lapse imagery from the full duration of the experiment, digital elevation models (DEMs) using structure for motion software, overhead images of a completely submerged sand bed to correlate water blueness to water depth, flow velocities over time using particle imaging velocimetry (PIV), and images of evolving morphology with a digital single-lens reflex camera. An overview of the data collection moments is given in supporting information Table S1.

Seven industrial CMOS MAKO color cameras were used to collect time-lapse imagery from the experiment. The resolution of each camera was 2,048 by 2,048 pixels, and they had a fixed focal length of 12.5 mm, which resulted in a spatial pixel resolution of 1.5–2 mm. The cameras were installed 3.7 m above the centreline of the flume, equally spaced. Each tidal cycle, images were taken when the flume was in horizontal position at the onset of the flood flow. Because the camera alignment was hampered by the roof supports in the lab, the images were orthorectified and corrected for vignetting and lens distortion. Subsequently, images were stitched and converted to LAB (CIELAB) images. Extraction of the B-band enhanced the visualization of morphology thanks to the contrast between the blue colored water and yellowish sediment.

Fluorescent light with daylight color was directed at a white diffusive ceiling from about 4.5 m above the flume floor. This setup resulted in an illumination of about 300 lux. We largely prevented the reflection of light from the water surface by installing white backdrop cloth between the light source and the flume, which reduced the intensity of the light and made it more diffuse, but could not prevent reflection of the support beams of the roof. The light intensity allows for low exposure times, which was used for PIV.

DEMs were obtained using structure from motion software (Agisoft, 2017; Chandler et al., 2001; Fonstad et al., 2013; Lane et al., 1993; Morgan et al., 2017). To this end, a digital single-lens reflex (DSLR) camera was mounted on a pole, which was stabilized on a bridge that rolled on the flume walls. Photographs were taken slightly inclined to the flume at equal spacings along the flume. 20 ground control points, located on the inner side of the flume walls, were used as references for the DEMs. The referencing allowed for resampling of DEMs on the same grid as used for the stitched time-lapse imagery.

PIV (Mori & Chang, 2003) was used to measure flow velocities over a tidal cycle. First, we seeded white polystyrene particles (diameter approximately 2.5 mm) on the water surface. Second, in 16 phases of the tide, a frequency generator triggered the collection of ten images at 25 Hz, simultaneously by all overhead cameras. Particles were resupplied where and when necessary. Third, images were corrected for illumination with background imagery without particles. Last, flow velocities were calculated from each pair of consecutive images using the MPIV toolbox in Matlab (Mori & Chang, 2003). The peak cross-correlation algorithm was used to obtain average displacement of particles in a 50×50 pixel window with overlap of 50%. Subsequently, the vector fields with displacement in pixels per second were scaled by the camera footprint. The camera footprint (1.5–2 mm/pixel) was calculated based on the flume geometry, average height of cameras, camera resolution and the instantaneous tilting angle. Erroneous vectors resulted from windows that were partially filled with flume wall, spots empty of particles or over seeded with particles, mismatched particles and reflections on the water surface. For further processing and analysis, we calculated the average vector field from each set of ten consecutive images. Flow velocity data was also interpolated on the same grid as used for DEMs and time-lapse imagery.

Water depth was estimated from overhead imagery. To be able to correlate the blueness from overhead imagery with water depth, the sediment bed was fully submerged, after which overhead images were taken. Subsequently, a DEM was made for the same state of the sediment bed. A correlation of these two resulted in a predictive relation for water depth (m) as a function of blueness (b; on a scale from 0 to 1 for the B-band of LAB images): $h = 7.0 \times 10^{-6} \mathrm{b}^{-11} + 0.01$ (supporting information Figure S2). The correlation was applied to the background images collected during PIV to obtain time series of water depth with full coverage of the flume. In theory, water depth could subsequently be added to the bed elevation from DEMs to obtain the water surface elevation. However, because the uncertainty in DEMs (approximately 1.0 mm) and correlation between blueness and water depth (approximately 1–5 mm) is within the range of cross-channel differences in water surface elevation, we only use this method to estimate water depth variation over a tidal cycle. To

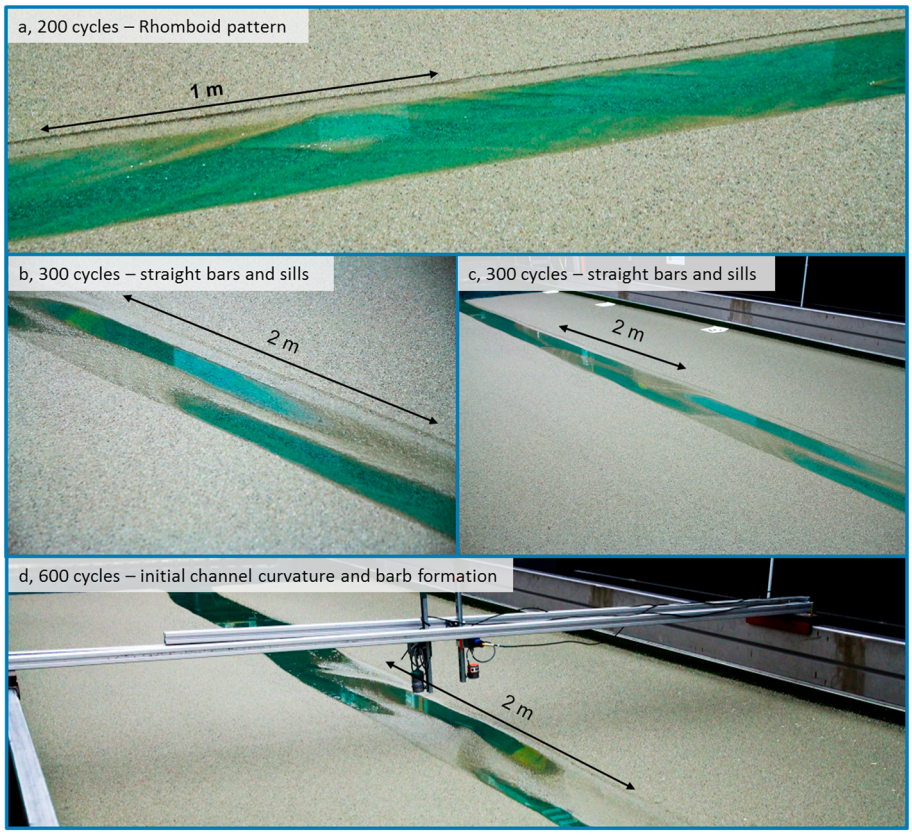

Figure 3. Digital single-lens reflex photography of the morphology in experiment 017. Except for panel (a), photographs were taken at a water level lower than mean sea level by draining the flume to enhance the visibility of morphology. (a) Initial rhomboid pattern with a characteristic wavelength in the order of centimeters. (b, c) Alternate bars with a bar length of approximately 0.5–0.7 m separated by straight, narrow, and elongated sills. (d) Initial channel curvature and the formation of U-shaped lobate bars in channels with opposing flow.

study flow around sills, flow velocities were also filtered along the thalweg: in the channel, seaward of the sill, on top of the sill and landward of the sill.

2.3. Data Reduction

The following characteristics were derived from DEMs: estuary width, cross-sectional area, summed width of bars, bar length, bar width, and BI. Estuary width was calculated as the width between the noneroded banks including the sand bars. Cross-sectional area was calculated as the total area below the plane sediment bed.

To calculate the characteristics of bar pattern, first, the bathymetry was converted into a binary image of channels and bars. To do so, median bed level was calculated per cross section and subsequently a linear fit was used as the threshold between channel and bar. From the classified bar map, the summed width of bars was calculated per cross section. BI was calculated as the number of channels plus bars divided by two. The characteristic bar width was calculated as the summed width of bars divided by the BI. Bar length was calculated as the length between two successive inflection points in the along-channel profile of summed width of bars. All characteristics were averaged along the entire flume to obtain characteristic values of bar pattern per time step.

To obtain characteristic hydrodynamic conditions for specific morphological features, we classified channels in the following categories: tip of the ebb channel, ebb channel, straight channel, flood channel, and tip of the flood channel (supporting information Figure S3). Ebb and flood channels were recognized as channels with a dead end in one of the flow directions. In contrast to the channels, the tips were chosen on the shallowest part of either the ebb or flood barb, while ebb and flood channels were chosen well within the

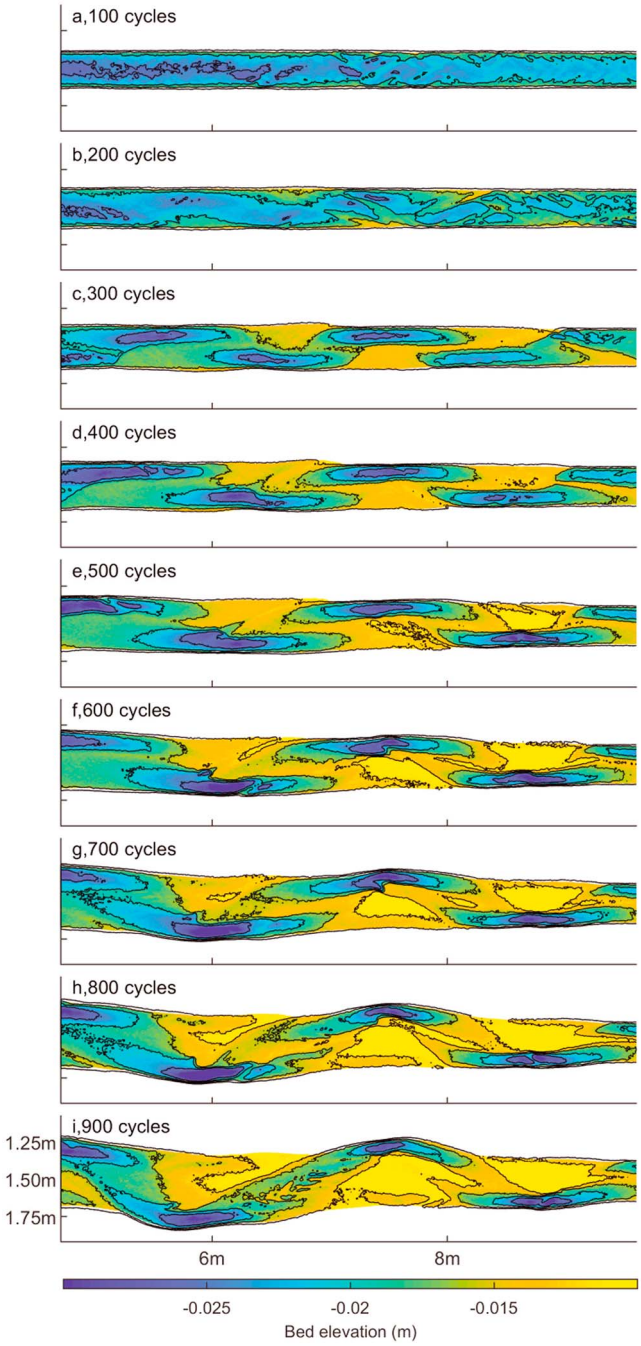

Figure 4. Incipient bar pattern formation in an experiment with open boundaries on both sides. Contours are drawn at −4, −12, −20, and −28 mm with respect to the 0-mm reference level of the erodible sand bed. (a–c) Distinguishable channels and bars formed after 300 cycles. Channels remained straight until approximately 500 cycles (e). From that moment onward, channels became more curved and braiding index increases (f–i). Elevation of sand bars increased over time in the zone from 6–9 m. Typical bar length only slightly increased after their initial formation.

channel. Straight channel was assigned to the part of the channel that was in the middle between the ebb barb and flood barb in a straight channel, typically at the deepest location.

3. Results

First, the phases of incipient bar formation are described along with their dependency on initial channel geometry. Second, we quantify the bar patterns. Last, we study the hydrodynamic conditions that lead to the observed morphology.

3.1. Phases of Incipient Bar Formation

The experiments showed three characteristic steps in incipient tidal bar formation. First, a rhomboid pattern evolved, which is a series of parallel short and narrow ridges that are oblique with respect to the channel orientation (Figures 3a and 4a). Second, alternate bars grew with a bar length of approximately 0.6–0.7 m within 300 cycles (Figures 3b, 3c, and 4c). Initially, straight channels formed U-shaped lobate bars in both the ebb and flood direction (supporting information Figure S5). Two opposing U-shaped bars on the same side of the estuary amalgamated into an alternate bar and the channel on the opposite side of the estuary eroded the side of the alternate bar. Narrow and straight sills were superimposed on and connected successive alternate bars, separating straight tidal channels that were 1–2 m long. This resulted in deepest channels flanking alternate bars rather than occurring between the bars. Typical bed level profiles resulting from alternate bar and sill formation are shown in Figure 5. Lastly, the ebb-dominated ends of channels formed U-shaped lobate bars in the opposing flood tidal channels and vice versa (300–600 cycles; Figures 3d and 4d–4f), which resulted in continuous outer-bend erosion and migration of the channels toward the sides of the estuary. From that time onward, the opposing channels were pushed sideways, eroding the banks, which allowed for bars to widen (Figures 4e–4i). This effect was possibly strengthened because flow from one channel into the other caused flow oblique to the thalweg, that is, directed toward the outer bend, eroding the bank (supporting information Movie S1). Outer meander bends migrated both laterally as well as in seaward direction. Seaward migration speed of outer bends decreased with distance from nearest mouth (Figure 6).

The initial phase was similar in all experiments, including the experiments with a wider straight channel. Experiments with a wide and straight initial channel (0.6 m) lacked the second phase that was observed in the narrower (0.2 m) channel. The channel mainly deepened along the channel axis in the initially wide channel, compared to side deepening in the narrow channel (Figure 7). This became apparent from the deepest channel forming in the middle of the initial channel rather than on the side (Figures 7b and 7c). Moreover, midchannel bars started growing at the beginning of the experiment (Figures 7b and 7c) but were later eroded away as a single meandering channel with alternate bars and a few barb channels formed (Figure 7g). These bars were longer and wider compared to the experiment with a narrow channel (Figure 7g,n).

Narrow and straight sills formed between successive alternate bars (Figure 3b). Although their morphology formed discrete, recognisable elements in images taken while draining the flume (Figure 3), their presence is less recognisable from overhead imagery and bathymetry because their elevation was typically low and they were less pronounced compared to the surrounding bars and channels. Nevertheless, the sills remained

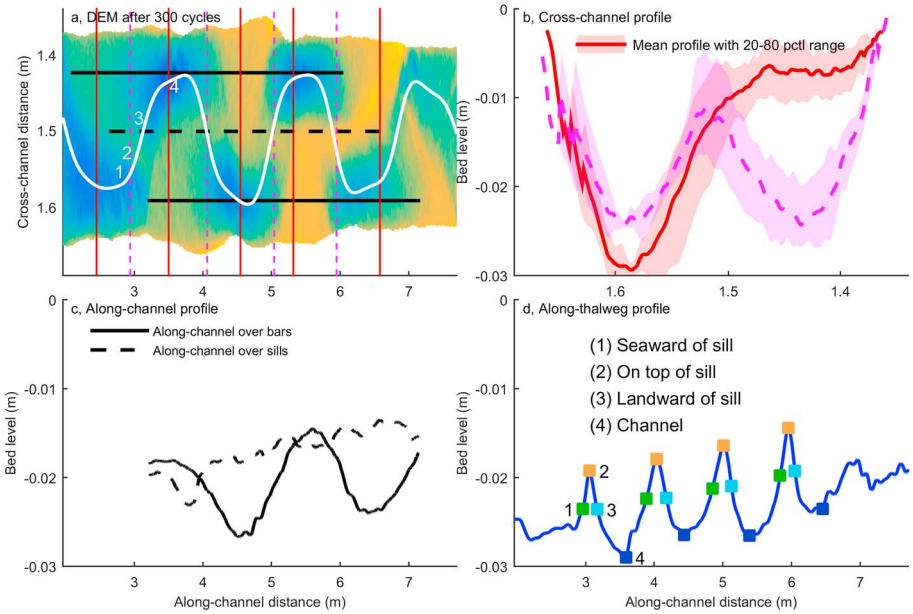

Figure 5. (a) Bathymetry after 300 cycles with the location of along-channel (black), cross-channel (red), and along-thalweg (white) profiles. Color scale is equal to Figure 4. (b) Cross-channel profiles of bed level at bar locations (red solid) and at sill locations (pink dashed). Bed levels were detrended with the along-channel gradient before calculating the average channel profile. Shaded area indicates 20th to 80th percentiles. (c) Along-channel profiles of bed level over the channels and bars (solid) and over the sills and bars (dashed). (d) Along-thalweg profile of bed level. Colored squares indicate the locations where flow velocities were extracted from PIV in Figure 10a.

present after the phase of incipient tidal bars and channels. For example, contour lines indicate the presence of the sill at 8 m (Figures 4f–4i), which grew in height, disconnected from the bar located at 9 m (Figures 4f and 4g) and migrated seaward to merge with the bar that formed at 7.5 m (Figures 4h and 4i).

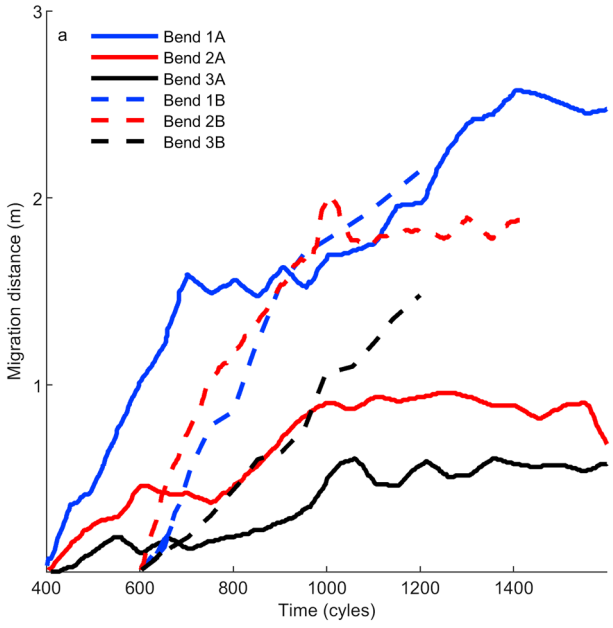

Figure 6. Meander bend migration over time. Initial position of meander bends are indicated in Figure 14d. Solid lines indicate bends on the left side of the flume, dashed lines on the right side. Bends on the right side started migrating 200 cycles later than on the left side.

While not accentuated by contour lines, the sills also remained present at the other locations along the flume (e.g., at 5.5 and 6.5 m; Figure 4i). In all cases, their orientation became oblique to the centreline of the flume and they were enclosed by opposing ebb and flood tidal channels. The elevation of the sills and bars increased with distance from the sea. However, only in the zone around 7–9 m, sill height approached bar height.

3.2. Quantified Bar Pattern: Channel and Bar Dimensions and BI

Average estuary width increased about linearly during the initial phase of the experiment (Figure 8b). Experiments that were run for a longer period of time (15,000 cycles, Leuven et al., 2018b) showed that channel widening decreased over time but continued until flume walls were reached. Only with the addition of cohesive material (Braat et al., 2019) estuary widening was inhibited, because cohesive material fills up intertidal area and thereby reduces the tidal prism that otherwise continues to increase. Average estuary depth initially decreased but stabilized on the longer term (Figure 8b). Bar length and BI increased with increasing estuary width (Figures 8a and 8b). For bar length, scatter and along-channel variation was relatively large, but average values suggest that it kept increasing. The same holds for BI. Bar width stabilizes in the first 1,000 cycles of the experiment at about 0.2 m (Figure 8a).

Along-channel profiles revealed considerable spatial variation in estuary width, bar width, minimum bed elevation, and cross-sectional area (Figure 9). The initial widening was nearly constant along-channel, but

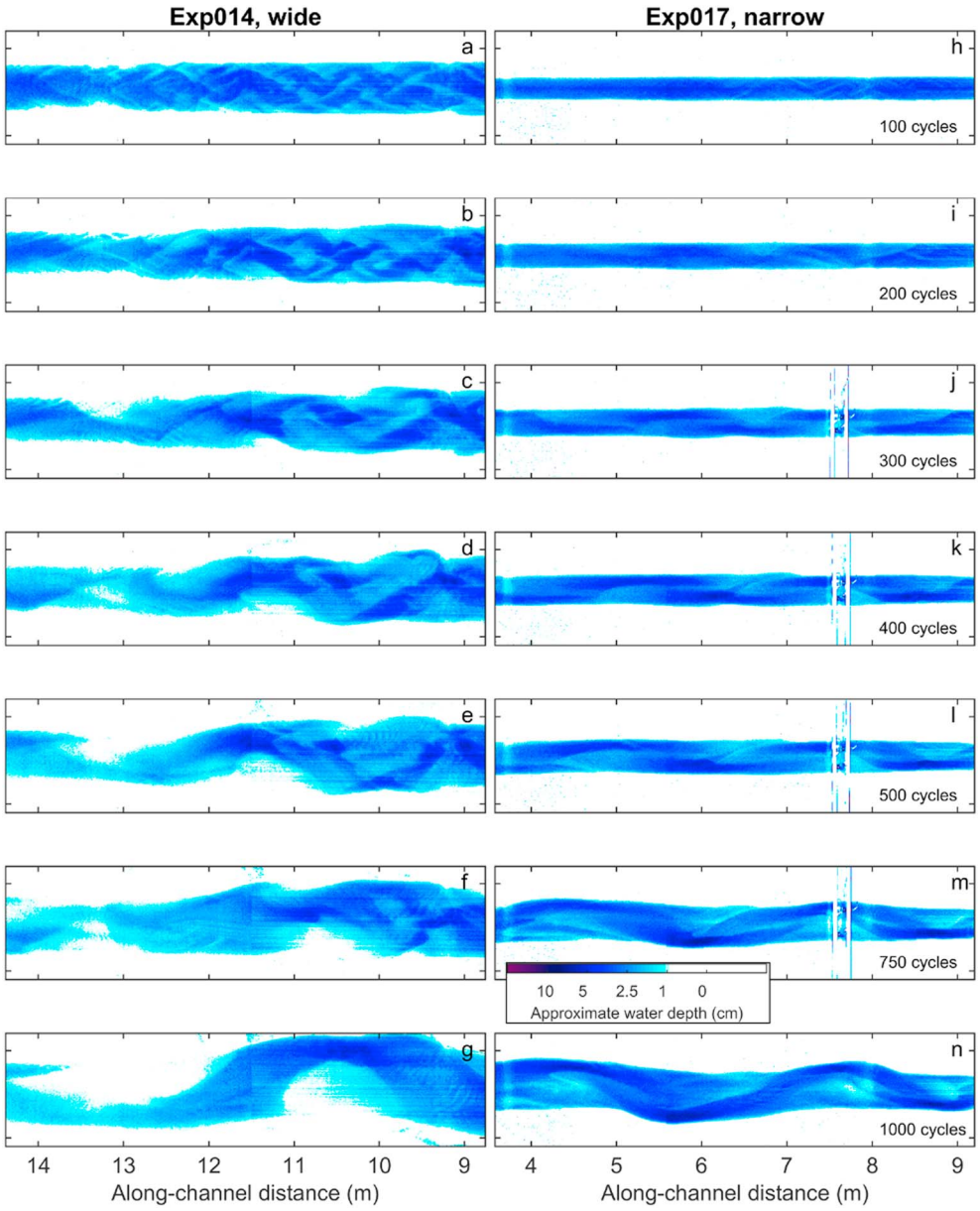

Figure 7. Time series of overhead imagery of experiment 014 and 017. Time steps are indicated in the right panel. The color bar indicates the approximate conversion between blueness and water depth (see also supporting information Figure S2). In both cases, the initial phase is characterised by a rhomboid pattern, followed by an alternate bar pattern (see also Figure 3). In later phases, channels become more curved and braiding index increases due to the formation of barb channels.

in later phases the width profile became progressively more irregular (Figures 9b and 9c). Profiles of minimum bed elevation, that is, maximum depth, illustrate that the bed profile was linearly sloped in the seaward direction during the first stages of the experiment (Figure 9e). However, with the onset of alternate bar formation, deep channels formed scours sideways of the alternate bars. This resulted in an along-channel elevation profile with quasiperiodic variation related to the length scales of the bars (Figures 9b and 9e). The resulting cross-sectional area profile evolved from initially near linear to progressively more irregular (Figure 9f), due to the aforementioned changes in width and depth.

3.3. Residual Flow and Sediment Recirculation

In general, peak flood velocities were slightly larger than peak ebb velocities over the entire length of the experiments and both decreased over time (Figure 8c). Peak flow velocities rapidly decreased from

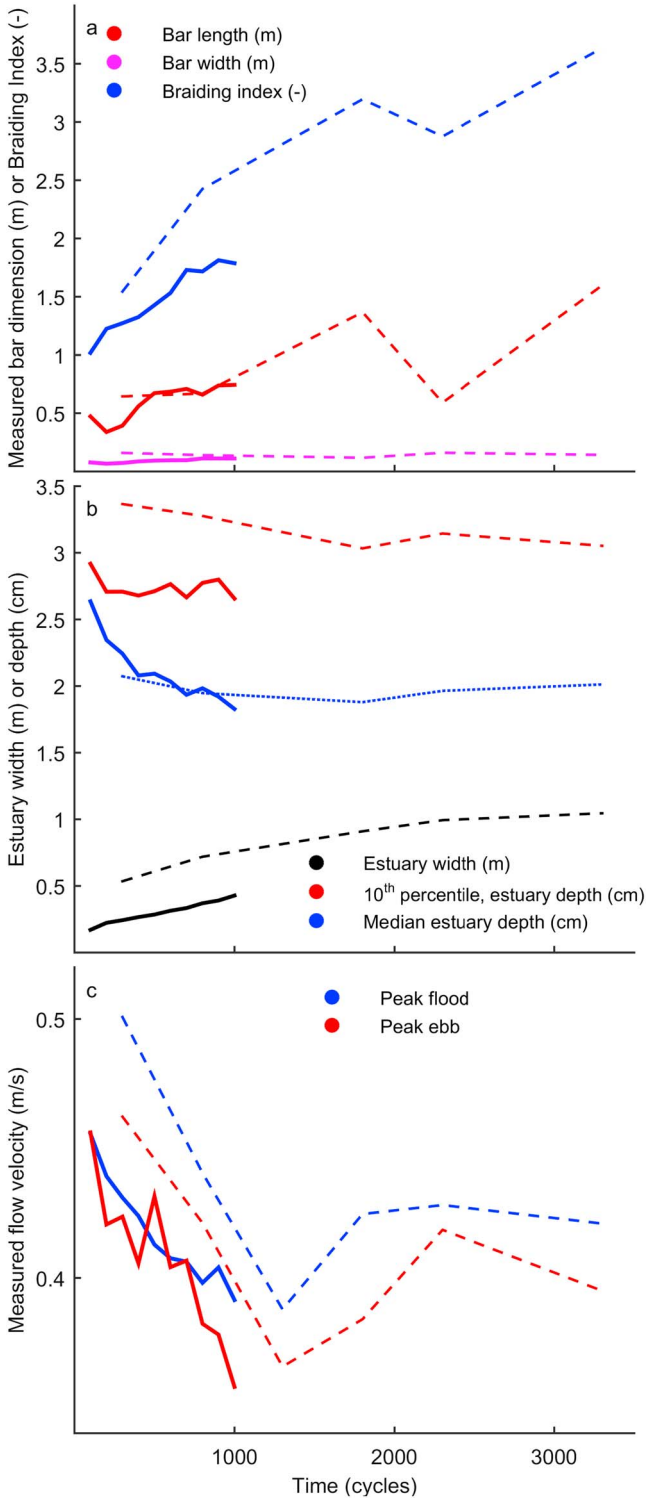

Figure 8. (a) Bar dimensions and braiding index, (b) estuary dimensions, and (c) peak flow velocity over time for Exp. 006 (dashed lines) and Exp. 017 (solid lines). Bar dimension and braiding index are along-channel averaged values. Average estuary width is larger for Exp. 006, because the experiment started with an initial converging channel that was much wider at the seaward boundary than the straight channel of Exp. 017 (Figure 2). Exp. 006 was a previous experiment (Leuven et al., 2018b) with one closed boundary and an initial converging channel, shown here for comparison. Characteristic estuary depth was calculated as the 10th percentile and median value. Peak flow velocities are the 5th and 95th percentile values.

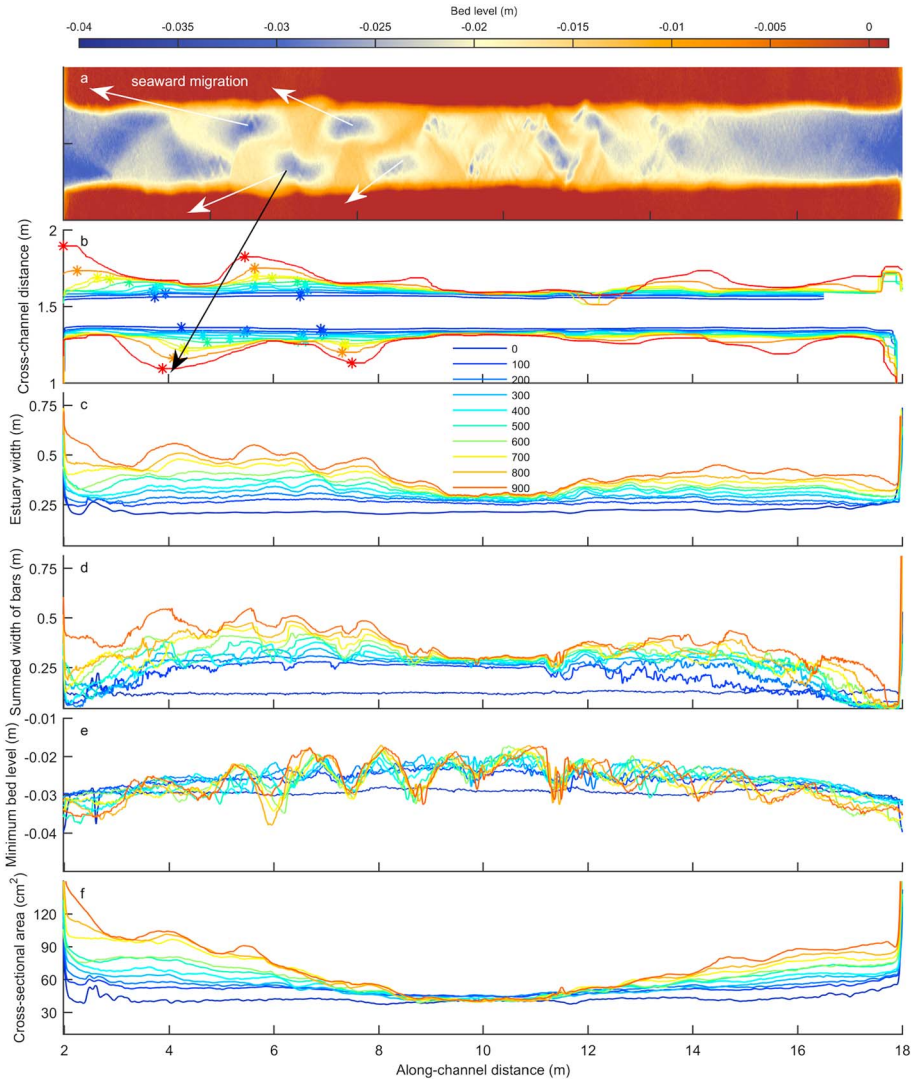

Figure 9. (a) Bathymetry after 300 tidal cycles. Along-channel profiles of (b) estuary bank location, (c) estuary width, (d) summed width of bars, (e) minimum bed elevation, and (f) cross-sectional area over time in the experiment with a narrow channel. The white arrows in panel (a) indicate migration direction of initial channels, resulting in specific zones where the estuary widened in panels (b) and (c). Asterisks indicate maximum lateral bank erosion per time step (see for enlarged version supporting information Figure S4).

approximately 0.45–0.50 m/s to 0.35–0.40 m/s in the first 1,000 cycles, after which they became more constant. Flow conditions obey to the most important scaling rules as indicated by sediment mobility being above the threshold for motion for the largest part of the tidal cycle and flow being subcritical and turbulent for the entire tidal cycle (Figure 10). Typical values of these parameters for real estuaries are reported in Table 2 in Kleinhans, van der Vegt, et al. (2017).

Flow conditions, and especially flow divergence and convergence, are indicative of sediment transport in the experiment. The gradients observed in flow velocities and sediment mobility explain the formation and persistence of the straight sills located between the alternate bars. Flow divergence is already noticeable after 300 tidal cycles (supporting information Movie S1). Flow velocities at characteristic locations along the thalweg (i.e., main channel; Figure 5a) indicate that after peak flood the flow decelerates over the sill and accelerates again after the sill (Figure 10a), suggesting sediment convergence seaward of the sill. Over almost the entire ebb phase, flow decelerates landward of the sill (Figure 10a), with sediment being hardly mobile on top and landward of the sill (Figure 10b).

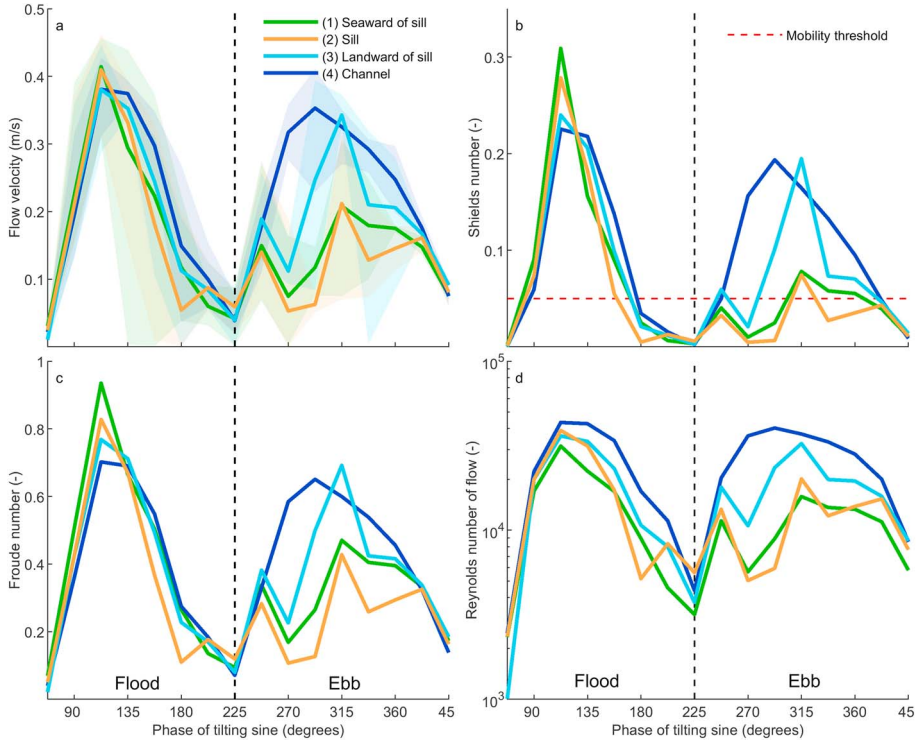

Figure 10. (a) Flow velocity over time for the locations indicated in Figure 5d. Velocity profiles were corrected for phase difference induced by the along-channel distance and averaged per class. Shaded areas indicate maximum and minimum per class. During both the ebb and the flood phase flow decelerates at the sills, which indicates flow divergence, especially in the second half of the flood phase and during the middle part of the ebb phase. (b) Shields number, (c) Froude number, and (d) Reynolds number over time calculated for the class averaged flow velocity. The dashed vertical line at 225° indicates the transition from flood flow to ebb flow.

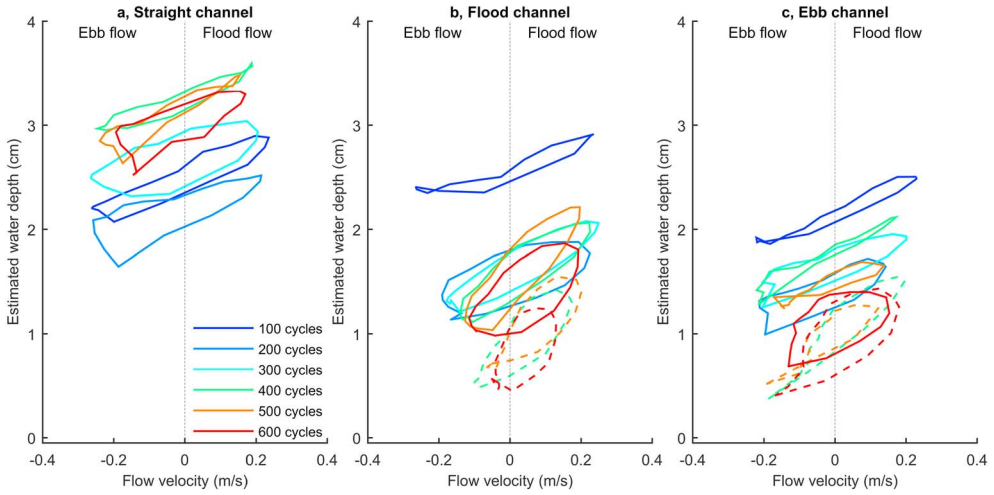

Figure 11. Tidal stage diagrams with water depth against flow velocity. Water depth was estimated from a calibration between blueness and bathymetry (supporting information Figure S2). Flow velocities were measured with Particle Image Velocimetry. Typical stage diagrams were obtained by averaging the measured values at characteristic locations along the flume: (a) center of straight channels, (b) flood channels (solid) and the bar tip of the flood channel (dashed), (c) ebb channels (solid), and the bar tip of the ebb channel (dashed).

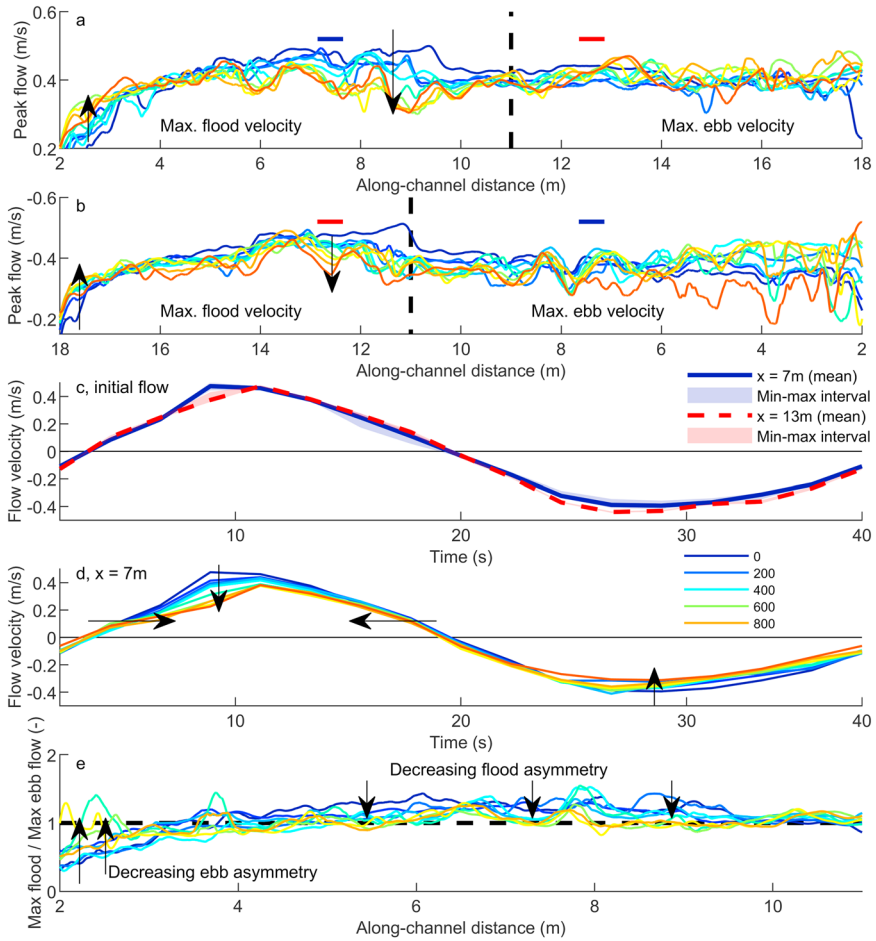

Figure 12. Flow velocity measurements in the experiment with a narrow channel (Exp. 017). Along-channel peak flow velocities for the flume tilted (a) to the right and (b) to the left. Colors indicate time in tidal cycles (legend in panel d). Dashed vertical line indicates the higher elevated part in the middle of the flume. (c) Tidal flow velocity at the beginning of the experiment at $x = 7$ m and $x = 13$ m. Measurement locations are indicated in panels (a) and (b) and shaded area indicates the minimum and maximum measured values. Peak flood flow is initially stronger than peak ebb flow on both sides of the flume. (d) Tidal flow asymmetry over time on the left-hand side of the flume. (e) Along-channel ratio of peak flood velocity divided by peak ebb velocity. Arrows indicate trends over time.

In the straight channels, water depth increased over time, while peak flow velocity decreased (Figure 11a). As expected, peak flood velocities are typically larger than peak ebb velocities in the flood channels, where peak ebb velocity decreased over time. While the average water depth remained fairly constant, the difference in water depth between the ebb and flood phase increased over time. Largest water depths coincided with peak flood velocities while peak ebb occurred just before lowest water levels, resulting in more inclined ellipses in the tidal stage diagrams (Figure 11b). In the ebb channels, peak ebb and flood velocity were initially approximately equal, but the tidal stage diagrams became progressively more ebb dominated (Figure 11c). Water depth in these channels kept decreasing over time. The tips of both ebb and flood channels were characterised by higher peak flood velocities than peak ebb velocities (dashed lines in Figures 11b and 11c). Elevation of the tips of both ebb and flood channels were typically the highest, thus explaining why the observed flow velocity and water depth were generally low during the ebb phase.

Initial flow conditions were similar on the left and right sides of the flume (Figures 12a–12c). Over time, asymmetry in peak ebb and peak flood velocity decreased (Figures 12a, 12b, and 12e). In the middle of the flume, peak flood velocities reduced, while in the seaward zone peak flood velocities increased (Figures 12a and 12b), likely due to landward shallowing and seaward deepening (Figure 9e). The flood duration decreased slightly over time, showing a more peaked profile than the ebb flow (Figure 12d).

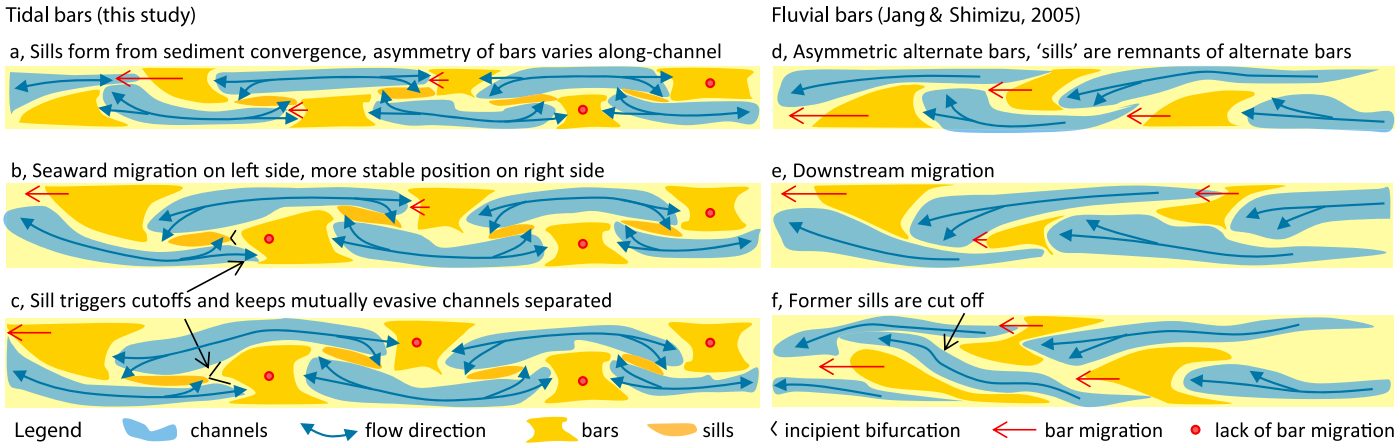

Figure 13. (a–c) Incipient tidal bar formation based on the experiments presented in this study compared to (d–f) incipient bar formation in rivers based on Jang and Shimizu (2005).

4. Discussion

4.1. Incipient Tidal Bar Formation

Mutually evasive ebb- and flood-dominated tidal channels are probably unique to the tidal environment (e.g., Dalrymple & Choi, 2007; Fenies & Faugères, 1998; van Veen, 1950). While past observations in natural systems suggested that mutually evasive ebb- and flood-dominated tidal channels are forced topographically by bends (Ahnert, 1960; van Veen, 1950), our experiments showed that stable sills initiate with the onset of tidal bar formation in the absence of topographical forcing. Sills arise spontaneously in a straight channel without topographical forcing, and the key mechanismr for sill formation between the alternate bars is as follows. Initially, the deepest channels form sideways of alternate bars rather than in between the alternate bars. Second, this configuration leads to flow divergence on both ends of the channels, causing convergence of sediment between the alternate bars, building up a sill (Figures 13a–13c). As such, sills are superimposed on the incipient bar and channel pattern. Sills persist over time and force the ebb and flood flow to take opposite paths around the sill over time. On longer timescales, this process modulates the sill, creating a preferential channel for flood and a preferential channel for ebb, also called mutually evasive ebb- and flood-dominated tidal channels (Figures 13a–13c).

The alternative hypothesis for sill formation by topographic forcing requires local width changes and channel curvature effects such as secondary circulation. While secondary circulation can exist in these shallow flows, the bend radius of the initially nearly straight channels was so large that secondary flow intensity was far too small to explain the observed sill slopes (see Figure 6 in van Dijk et al., 2013). Only in later phases, two opposing currents created lobate bars and oblique tidal currents that induced channel curvature around the sills (similar to Kleinhans et al., 2014). Only then the increased channel curvature (i.e., reduced bend radius) and estuary widening caused bars to become nonmigratory in the inner banks (also described by Frascati & Lanzoni, 2013; Repetto & Tubino, 2001; Repetto et al., 2002; Seminara, 2010; Zolezzi et al., 2012). At this stage the bars and sills became topographically forced, which is further evidence that the sills formed earlier are not topographically forced.

The sills also determine the location of future tidal bifurcations (Figures 13b and 13c) and thereby the long-term evolution of estuaries. As channel widening progresses, the flood channels initiate new channels on the alternate bars, forming barb channels (e.g., Hibma et al., 2003; Leuven et al., 2016; van Veen, 1950) and isolating midchannel bars. Subsequent diversion of flow around midchannel bars and localized bank erosion cause the quasiperiodic width variation observed along estuaries (Leuven et al., 2018b). Additionally, the estuary mouth widened very rapidly due to the sharp corners of the estuary banks at the mouth.

The evolution observed in our experiments is qualitatively in agreement with results from numerical models (e.g., Braat et al., 2017; Hibma et al., 2003, 2004; van der Wegen & Roelvink, 2008), other experiments (Tambroni et al., 2005) and observations in natural systems (Ahnert, 1960; Tank, 1996; van Veen, 1950). Numerical models of straight tidal basins with nonerodible banks also resulted in initially straight channels that later connected into a main meandering channel with flood barbs (Hibma et al., 2003, 2004; van der

Wegen & Roelvink, 2008). Conversely, numerical models (Braat et al., 2017) and experiments with erodible boundaries result in an initial phase of seaward migrating tidal bars and main meandering channels.

Linear stability theory (Schramkowski et al., 2002) correctly predicts the experimental observations that the BI of the initially fastest growing bar pattern increases with channel width. The setup with a wide channel showed initially a braided pattern, which later transitioned into an alternate bar pattern (Figure 7), consistent with earlier work (Dalrymple & Rhodes, 1995; Hibma et al., 2003; Tambroni et al., 2005, 2017). The experiments also showed that bar dimensions are initially smaller and that flow velocities are initially larger than in the phase of full-grown bars (Figure 8). This suggests that nonlinear effects are important for the dimensions of full-grown bars, highlighting the need of further development of nonlinear theory (Schramkowski et al., 2004).

4.2. Incipient Bar Formation in Estuaries and Rivers

Many of the morphological features and mechanisms observed in fluvial bar systems have a counterpart in tidal systems. A hierarchy of fluvial bars can be indicated by reference to unit bars and compound bars, independent of their shape and location, while the terms point bars, alternate bars, and midchannel bars refer to the shape or location where the bars occur (cf. Ashworth et al., 2000; Bridge, 1993, 2003; Cant & Walker, 1978; Kelly, 2006; Kleinhans & van den Berg, 2011; Rice et al., 2009; Sambrook Smith et al., 2006; Schuurman et al., 2013). Here we compare incipient morphological elements of rivers with those of tidal systems, as was previously done for fully grown bars in natural systems (Ashley, 1980; Dalrymple & Rhodes, 1995; Tank, 1996).

The alternate bar pattern observed during incipient tidal bar formation and in other tidal experiments (Tambroni et al., 2005, 2017) is very similar to alternate fluvial bars and was also observed in former scale experiments of rivers (Jang & Shimizu, 2005; van Dijk et al., 2012). Our experiments showed that, in contrast to rivers, alternate tidal bars are an amalgamation of two opposing U-shaped lobate bars, which makes them more symmetrical than river bars (Figure 13). However, in the seaward zone, where flow was typically more ebb dominated (Figure 12e), bars were more asymmetrical and thus more similar in shape and formative process to river bars (Figure 13).

Point bars are a shared in-channel element of tidal channels and rivers (Barwis, 1977; Bridges & Leeder, 1976; Brivio et al., 2016; Choi et al., 2004; Choi & Jo, 2015; de Mowbray, 1983; Ghinassi et al., 2018; Pearson & Gingras, 2006; Solari et al., 2002; Tank, 1996), but only in cases where the channel is relatively narrow and deep such that the active BI is unitary and where channel curvature is strong enough to force the bar to be nonmigratory. However, in the absence of bank strength the experiments showed behaviour similar to river braiding. Before point bars developed, the inner banks were cut-off by a progressively growing flood barb channel resulting in a midchannel bar. Previous experiments with cohesive suspended material that formed mud flats and floodplain (Braat et al., 2019) showed the evolution of a point bar in the landward portion of the estuary.

A characteristic element in gravel bed rivers is the "riffle-pool" sequence. Similar sequences of shallow sills and deeper channels have been observed in the Western Scheldt (Tank, 1996), in a meandering tidal channel (Dury, 1971) and in the experiments presented here, but the forming mechanism is probably different. Water level gradients above riffles in rivers are typically very large, which is not the case above sills in estuaries. Sills in estuaries differ from unit bars in rivers in their dynamic behavior. Unit bars migrate downstream until they amalgamate (e.g., Bridge, 1993; Schuurman et al., 2013), while sills in tidal systems are slaved to the larger-scale channel bar pattern as they are shaped by sediment convergence from the tidal channels (Figures 13a–13c).

4.3. Timescales of Tidal Bar Formation

Bar patterns in numerical models evolved over a period of 50–200 years (Hibma et al., 2003; van der Wegen & Roelvink, 2008), compared to approximately 1,000–3,000 tidal cycles in our experiments, which would correspond to 1–5 years in natural systems, assuming the same spatiotemporal scale factor. This implies that morphological evolution in our experiments is a factor 10–100 faster than in numerical models and in natural systems as also found for fluvial experiments (Kleinhans, Braudrick, et al., 2015). This is partly explained by complete lack of bank strength in experiments without vegetation and cohesive material (van Dijk et al., 2012), leading to an almost unlimited sediment supply, which immediately becomes available for bar formation downstream of the erosion location (van de Lageweg et al., 2014). This led to a strong increase in BI as

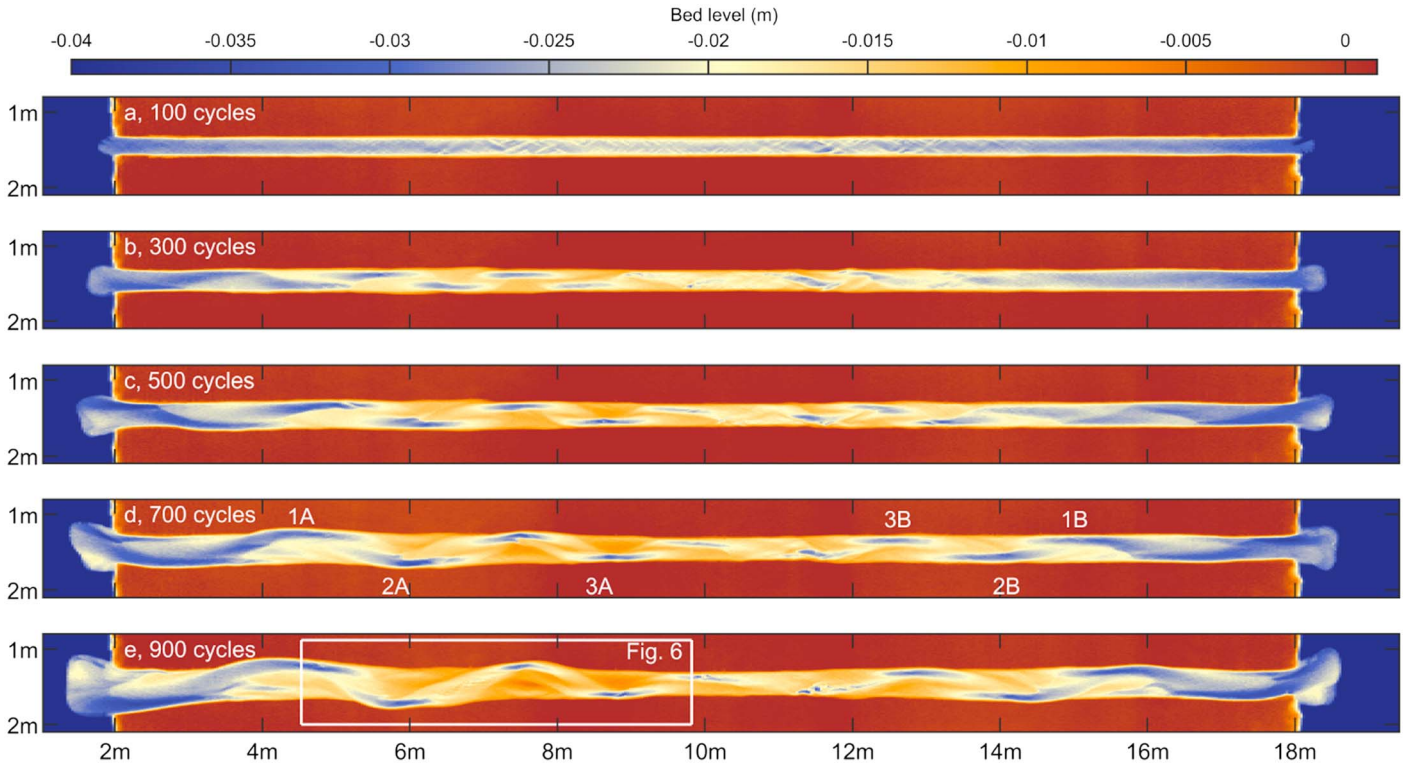

Figure 14. Time series of bathymetries obtained with structure from motion in the experiment with a narrow channel (Exp. 017). (a) Initially, the channel widened at an equal rate along the entire channel. (b) While incipient bars and channels developed, a relatively elevated zone formed in the middle of the flume (≈10–11 m). (c, d) In later phases, this higher elevated zone was the location where channel width remained narrow and widening ceased. (d, e) On both sides, two converging systems developed. The rate at which the channel widened, bars formed, channels became curved and braiding index increased, was faster for the left-hand side of the flume compared to the right-hand side of the flume.

the estuary widens, because average bar width remains constant at approximately 0.2 m. While bar growth in the experiments is unexpectedly fast, we lack observations in nature of initial bar formation and the timescale in the numerical models is highly sensitive to the chosen sediment transport relation, transverse bed slope effect, and numerical diffusion which renders the models unreliable indicators of morphological timescales without calibration.

The rate of morphological evolution correlates positive with the tidal prism (e.g., bend migration; Figure 6), which, in turn, depends on the location of the tidal watershed. This correlation is consistent with observations along tidal inlets (Kleinhans, Scheltinga, et al., 2015; Stefanon et al., 2010; Zhou et al., 2014) and tidal meanders (Finotello et al., 2018). Incipient bars and channels formed faster (in 300 cycles as opposed to 500 cycles) on the left-hand side (2–11 m) of the flume, which was also approximately 25% longer than the estuary on the right-hand side (11–18 m) of the flume. This either suggests that the initial sand bed was not sufficiently symmetrical or that the location of the tidal watershed is unstable and tends to shift as one watershed grows at the cost of the other in a positive feedback cycle. In reality this is unlikely to happen as the tidal wavelength is limiting the length dimension of tidal basins and estuaries (de Swart & Zimmerman, 2009; Schuttelaars & de Swart, 2000), but here we simulated a reach within a tidal system which allowed reasonable isolation of bar morphology from boundary effects.

The experimental setup with a double-head tidal channel led to the formation of two rather separated estuarine systems. The sediment eroded from the estuary banks in the initial phase was partly exported to the sea and also partly accumulated in the middle part of the flume (at ≈10–11 m; Figure 14a). Peak flood flow was initially slightly stronger on both sides. The initial flood flow asymmetry and the erodible, sharp corners of the estuary banks at the mouth explain why sediment was imported to converge in the middle of the flume (Figure 9e). The higher elevated part formed an obstruction for the flow, reducing the exchange of discharge between the left side (2–11 m) and right side (11-18 m) of the flume. At that location channel width remained narrow, which over time resulted in two separate converging channels in both directions

of the flume (Figure 14e). The morphological evolution in the zone between 2 and 11 m was slightly faster than the evolution in the other part (11–18 m).

Even though we did not anticipate the formation of two separated estuarine systems, the formation of a shore-like morphology acting as a tidal divide is consistent with experimental and numerical observations (Garotta et al., 2008; Lanzoni & Seminara, 2002; Schuttelaars & de Swart, 2000; Tambroni et al., 2017; van der Wegen & Roelvink, 2008). We chose the setup of a double-headed tidal channel (e.g., Dury, 1971; Hughes, 2012) aiming to create symmetrical reversing uniform flow along the entire flume. Uniform flow would allow studying bar formation independent of location along the flume, but unfortunately these conditions were only approximately met before bar initiation. It is therefore recommended to fixate the estuary banks for further research on bar initiation, and to explore the stability of tidal watersheds in upstream connected estuaries.

5. Conclusions

Laboratory-scale experiments were performed to study incipient bar formation under varying initial and boundary conditions. The resulting evolution of tidal bars was similar among experiments and qualitatively in agreement with previous results from numerical modeling and observations in natural systems. After an initial phase characterized by the formation of rhomboid depositional patterns with very short wavelength and high BI, straight initial channels formed with alternate bars. The deepest channels occurred sideways of the alternate bars while shallower zones formed in the crossovers between the alternate bars. This configuration led to flow divergence on both opposing ends of the channels, causing sediment convergence between alternate bars. Sediment convergence resulted in the buildup of elongated sills parallel to the main flow direction and located between alternate bars. This pattern is superimposed on the alternate bar and channel pattern and is unique to tidal systems. Even under asymmetric flow conditions the sills persisted. Their stable presence triggered the formation of mutually evasive ebb- and flood-dominated channels that bifurcate around the sill. As channel widening progressed, flood barbs formed onto the alternate bars, which in later phases resulted in midchannel bars and a braided pattern.

Incipient tidal bars are similar to river bars in their morphological shapes and their response to increasing width-to-depth ratio. The key differences are the process of alternate bar formation—by amalgamation of two opposing U-shaped lobate bars—and the formation and stable presence of the sill. Bar dimensions and BI were predominantly correlated with estuary width and lacked dependence on channel depth and amplitude of tidal flow velocity. Observations in natural systems may have suggested that mutually evasive ebb- and flood-dominated tidal channels are topographically forced, but here we showed that their stable presence is initiated with the onset of tidal bar formation and thus does not necessarily require topographical forcing.

Acknowledgments
This research was supported by the Dutch Technology Foundation TTW (grant Vici 016.140.316/13710 to M. G. K.), which is part of the Netherlands Organisation for Scientific Research (NWO), and is partly funded by the Ministry of Economic Affairs. This work is part of the PhD research of J. R. F. W. L. We are grateful for technical support by Marcel van Maarseveen, Henk Markies, Arjan van Eijk, Mark Eijkelboom, and Bas van Dam. We acknowledge a data processing contribution by Thijs de Lange as part of his MSc research. Discussion with Steven Weisscher helped to improve the manuscript. Constructive reviews by Alvise Finotello, Howard Feldman, and one anonymous reviewer, and steer by the Editor and Associate Editor helped to improve the manuscript. Author contributions: J. R. F. W. L. performed experiments, collected and analyzed data, and wrote the manuscript, M. G. K. contributed to conception and design and writing the manuscript. The data used are listed in the references, figures, and supporting information. The authors declare that they have no conflict of interest.

References

Agisoft (2017). Agisoft photoscan.
Ahnert, F. (1960). Estuarine meanders in the chesapeake bay area. *Geographical Review*, *50*, 390–401. https://doi.org/10.2307/212282
Ashley, G. M. (1980). Channel morphology and sediment movement in a Tidal River, Pitt River, British Columbia. *Earth Surface Processes*, *5*(4), 347–368. https://doi.org/10.1002/esp.3760050406
Ashmore, P. E. (1982). Laboratory modelling of gravel braided stream morphology. *Earth Surface Processes and Landforms*, *7*(3), 201–225. https://doi.org/10.1002/esp.3290070301
Ashworth, P. J., Best, J. L., Roden, J. E., Bristow, C. S., & Klaassen, G. J. (2000). Morphological evolution and dynamics of a large, sand braid-bar, Jamuna River, Bangladesh. *Sedimentology*, *47*(3), 533–555.
Barwis, J. H. (1977). Sedimentology of some south carolina tidal-creek point bars, and a comparison with their fluvial counterparts. *Fluvial Sedimentology*, *5*, 129–160.
Bolla Pittaluga, M., Coco, G., & Kleinhans, M. G. (2015). A unified framework for stability of channel bifurcations in gravel and sand fluvial systems. *Geophysical Research Letters*, *42*, 7521–7536. https://doi.org/10.1002/2015GL065175
Braat, L., Leuven, J. R. F. W., Lokhorst, I. R., & Kleinhans, M. G. (2019). Effects of estuarine mudflat formation on tidal prism and large-scale morphology in experiments. *Earth Surface Processes and Landforms*, *44*(2), 417–432. https://doi.org/10.1002/esp.4504
Braat, L., van Kessel, T., Leuven, J. R. F. W., & Kleinhans, M. G. (2017). Effects of mud supply on large-scale estuary morphology and development over centuries to millennia. *Earth Surface Dynamics*, *5*(4), 617–652. https://doi.org/10.5194/esurf-5-617-2017
Bridge, J. S. (1993). The interaction between channel geometry, water flow, sediment transport and deposition in braided rivers. *Geological Society, London, Special Publications*, *75*(1), 13–71.
Bridge, J. (2003). *Rivers and floodplains*. Malden, Mass: Blackwell Publishing.
Bridges, P. H., & Leeder, M. R. (1976). Sedimentary model for intertidal mudflat channels, with examples from the Solway Firth, Scotland. *Sedimentology*, *23*(4), 533–552. https://doi.org/10.1111/j.1365-3091.1976.tb00066.x

Brivio, L., Ghinassi, M., D'Alpaos, A., Finotello, A., Fontana, A., Roner, M., & Howes, N. (2016). Aggradation and lateral migration shaping geometry of a tidal point bar: An example from salt marshes of the Northern Venice Lagoon (Italy). *Sedimentary Geology*, *343*, 141–155. https://doi.org/10.1016/j.sedgeo.2016.08.005

Cant, D. J., & Walker, R. G. (1978). Fluvial processes and facies sequences in the sandy braided South Saskatchewan River, Canada. *Sedimentology*, *25*(5), 625–648.

Chandler, J. H., Shiono, K., Rameshwaren, P., & Lane, S. N. (2001). Measuring flume surfaces for hydraulics research using a Kodak dcs460. *The Photogrammetric Record*, *17*(97), 39–61.

Choi, K. S., Dalrymple, R. W., Chun, S. S., & Kim, S.-P. (2004). Sedimentology of modern, inclined heterolithic stratification (IHS) in the macrotidal Han River Delta, Korea. *Journal of Sedimentary Research*, *74*(5), 677–689. https://doi.org/10.1306/030804740677

Choi, K., & Jo, J. H. (2015). Morphodynamics of tidal channels in the open coast macrotidal flat, southern Ganghwa Island in Gyeonggi Bay, West Coast of Korea. *Journal of Sedimentary Research*, *85*(6), 582–595. https://doi.org/10.2110/jsr.2015.44

Crosato, A., & Mosselman, E. (2009). Simple physics-based predictor for the number of river bars and the transition between meandering and braiding. *Water Resources Research*, *45*, W03424. https://doi.org/10.1029/2008WR007242

Dalrymple, R. W., & Choi, K. (2007). Morphologic and facies trends through the fluvial–marine transition in tide-dominated depositional systems: A schematic framework for environmental and sequence-stratigraphic interpretation. *Earth-Science Reviews*, *81*(3), 135–174. https://doi.org/10.1016/j.earscirev.2006.10.002

Dalrymple, R. W., & Rhodes, R. N. (1995). Estuarine dunes and bars. *Geomorphology and Sedimentology of Estuaries*, *53*, 359–422.

de Haas, T., Pierik, H., van der Spek, A., Cohen, K., van Maanen, B., & Kleinhans, M. (2017). Holocene evolution of tidal systems in the netherlands: Effects of rivers, coastal boundary conditions, eco-engineering species, inherited relief and human interference. *Earth-Science Reviews*, *177*, 139–163. https://doi.org/10.1016/j.earscirev.2017.10.006

de Mowbray, T. (1983). The genesis of lateral accretion deposits in recent intertidal mudflat channels, solway firth, Scotland. *Sedimentology*, *30*(3), 425–435. https://doi.org/10.1111/j.1365-3091.1983.tb00681.x

de Swart, H., & Zimmerman, J. (2009). Morphodynamics of tidal inlet systems. *Annual Review of Fluid Mechanics*, *41*, 203–229.

Dury, G. (1971). Channel characteristics in a meandering tidal channel: Crooked river, florida. *Geografiska Annaler: Series A, Physical Geography*, *53*(3-4), 188–197. https://doi.org/10.1080/04353676.1971.11879844

Eaton, B. C., Church, M., & Davies, T. R. (2006). A conceptual model for meander initiation in bedload-dominated streams. *Earth Surface Processes and Landforms: The Journal of the British Geomorphological Research Group*, *31*(7), 875–891. https://doi.org/10.1002/esp.1297

Eke, E. (2014). Numerical modeling of river migration incorporating erosional and depositional bank processes (Ph.D. thesis), University of Illinois at Urbana-Champaign.

Fenies, H., & Faugères, J.-C. (1998). Facies and geometry of tidal channel-fill deposits (Arcachon Lagoon, SW France). *Marine Geology*, *150*(1-4), 131–148. https://doi.org/10.1016/S0025-3227(98)00049-8

Finotello, A., Lanzoni, S., Ghinassi, M., Marani, M., Rinaldo, A., & D'Alpaos, A. (2018). Field migration rates of tidal meanders recapitulate fluvial morphodynamics. *Proceedings of the National Academy of Sciences of the United States of America*, *115*(7), 1463–1468. https://doi.org/10.1073/pnas.1711330115

Fonstad, M. A., Dietrich, J. T., Courville, B. C., Jensen, J. L., & Carbonneau, P. E. (2013). Topographic structure from motion: A new development in photogrammetric measurement. *Earth Surface Processes and Landforms*, *38*(4), 421–430.

Frascati, A., & Lanzoni, S. (2013). A mathematical model for meandering rivers with varying width. *Journal of Geophysical Research: Earth Surface*, *118*, 1641–1657. https://doi.org/10.1002/jgrf.20084

Fujita, Y., & Muramoto, Y. (1985). Studies on the process of development of alternate bars. *Bulletin of the Disaster Prevention Research Institute*, *35*(3), 55–86.

Garotta, V., Bolla Pittaluga, M., & Seminara, G. (2006). On the migration of tidal free bars. *Physics of Fluids*, *18*(9), 96601. https://doi.org/10.1063/1.2221346

Garotta, V., Rummel, A. C., & Seminara, G. (2008). Long-term morphodynamics and hydrodynamics of tidal meandering channels, *River, coastal and estuarine morphodynamics conference* (pp. 163–168). Enschede: Taylor and Francis/Balkema.

Ghinassi, M., Brivio, L., D'Alpaos, A., Finotello, A., Carniello, L., Marani, M., & Cantelli, A. (2018). Morphodynamic evolution and sedimentology of a microtidal meander bend of the venice lagoon (italy). *Marine and Petroleum Geology*, *96*, 391–404. https://doi.org/10.1016/j.marpetgeo.2018.06.011

Hibma, A., De Vriend, H., & Stive, M. (2003). Numerical modelling of shoal pattern formation in well-mixed elongated estuaries. *Estuarine, Coastal and Shelf Science*, *57*(5), 981–991.

Hibma, A., Schuttelaars, H., & de Vriend, H. (2004). Initial formation and long-term evolution of channel–shoal patterns. *Continental Shelf Research*, *24*(15), 1637–1650. https://doi.org/10.1016/j.csr.2004.05.003

Hijma, M. P., & Cohen, K. M. (2011). Holocene transgression of the rhine river mouth area, the netherlands/southern north sea: Palaeogeography and sequence stratigraphy. *Sedimentology*, *58*(6), 1453–1485.

Hughes, Z. J. (2012). Tidal channels on tidal flats and marshes, *Principles of tidal sedimentology* (pp. 269–300). Dordrecht: Springer. https://doi.org/10.1007/978-94-007-0123-6_11

Ikeda, H. (1973). A study on the formation of sand bars in a experimental flume. *Geographical Review of Japan*, *46*(7), 435–451.

Jang, C.-L., & Shimizu, Y. (2005). Numerical simulations of the behavior of alternate bars with different bank strengths. *Journal of Hydraulic Research*, *43*(6), 596–612. https://doi.org/10.1080/00221680509500380

Kelly, S. (2006). Scaling and hierarchy in braided rivers and their deposits: Examples and implications for reservoir modelling. *Braided Rivers: Process, Deposits, Ecology and Management (Special Publication 36 of the IAS)*, *21*, 75.

Kleinhans, M. G. (2010). Sorting out river channel patterns. *Progress in Physical Geography*, *34*(3), 287–326. https://doi.org/10.1177/0309133310365300

Kleinhans, M. G., Braudrick, C., Van Dijk, W. M., Van, W. I., de Lageweg, R., Teske, R., & Van Oorschot, M. (2015). Swiftness of biomorphodynamics in lilliput-to giant-sized rivers and deltas. *Geomorphology*, *244*, 56–73.

Kleinhans, M. G., Ferguson, R. I., Lane, S. N., & Hardy, R. J. (2013). Splitting rivers at their seams: Bifurcations and avulsion. *Earth Surface Processes and Landforms*, *38*(1), 47–61. https://doi.org/10.1002/esp.3268

Kleinhans, M. G., Leuven, J. R., Braat, L., & Baar, A. (2017). Scour holes and ripples occur below the hydraulic smooth to rough transition of movable beds. *Sedimentology*, *64*, 1381–1401.

Kleinhans, M. G., Scheltinga, R. T., Vegt, M., & Markies, H. (2015). Turning the tide: Growth and dynamics of a tidal basin and inlet in experiments. *Journal of Geophysical Research: Earth Surface*, *120*, 95–119. https://doi.org/10.1002/2014JF003127

Kleinhans, M., Van Rosmalen, T., Roosendaal, C., & van der Vegt, M. (2014). Turning the tide: Mutually evasive ebb-and flood-dominant channels and bars in an experimental estuary. *Advances in Geosciences*, *39*, 21–26.

Kleinhans, M. G., & van den Berg, J. H. (2011). River channel and bar patterns explained and predicted by an empirical and a physics-based method. *Earth Surface Processes and Landforms*, *36*(6), 721–738. https://doi.org/10.1002/esp.2090

Kleinhans, M. G., van der Vegt, M., Leuven, J., Braat, L., Markies, H., Simmelink, A., et al. (2017). Turning the tide: comparison of tidal flow by periodic sealevel fluctuation and by periodic bed tilting in the metronome tidal facility. *Earth Surface Dynamics Discussions*, *2017*, 1–35. https://doi.org/10.5194/esurf-2017-11

Lagasse, P., Zevenbergen, L., Spitz, W., & Thorne, C. (2004). *Methodology for predicting channel migration. NCHRP web-only document 67 (Project 24-16). National Cooperative Highway Research Program*. Washington, DC: Transportation Research Board.

Lane, S., Richards, K., & Chandler, J. (1993). Developments in photogrammetry: The geomorphological potential. *Progress in Physical Geography*, *17*(3), 306–328.

Lanzoni, S., & Seminara, G. (2002). Long-term evolution and morphodynamic equilibrium of tidal channels. *Journal of Geophysical Research*, *107*(C1), 3001. https://doi.org/10.1029/2000JC000468

Lentsch, N., Finotello, A., & Paola, C. (2018). Reduction of deltaic channel mobility by tidal action under rising relative sea level. *Geology*, *46*(7), 599–602. https://doi.org/10.1130/G45087.1

Leopold, L. B., & Wolman, M. G. (1957). *River channel patterns: Braided, meandering, and straight*. US: US Government Printing Office.

Leuven, J. R. F. W., Braat, L., van Dijk, W. M., de Haas, T., & Kleinhans, M. G. (2018b). Growing forced bars determine non-ideal estuary planform. *Journal of Geophysical Research: Earth Surface*, *123*, 2971–2992. https://doi.org/10.1029/2018JF004718

Leuven, J. R. F. W., Kleinhans, M. G., Weisscher, S. A. H., & van der Vegt, M. (2016). Tidal sand bar dimensions and shapes in estuaries. *Earth-Science Reviews*, *161*, 204–233. https://doi.org/10.1016/j.earscirev.2016.08.004

Leuven, J. R. F. W., van Maanen, B., Lexmond, B. R., van der Hoek, B. V., Spruijt, M. J., & Kleinhans, M. G. (2018a). Dimensions of fluvial-tidal meanders: Are they disproportionally large? *Geology*, *46*(10), 923–926. https://doi.org/10.1130/G45144.1

Lewin, J. (1976). Initiation of bed forms and meanders in coarse-grained sediment. *Geological Society of America Bulletin*, *87*(2), 281–285.

Morgan, J. A., Brogan, D. J., & Nelson, P. A. (2017). Application of structure-from-motion photogrammetry in laboratory flumes. *Geomorphology*, *276*, 125–143.

Mori, N., & Chang, K.-A. (2003). Experimental study of a horizontal jet in a wavy environment. *Journal of Engineering Mechanics*, *129*(10), 1149–1155.

Parker, G., Shimizu, Y., Wilkerson, G., Eke, E. C., Abad, J. D., Lauer, J., et al. (2011). A new framework for modeling the migration of meandering rivers. *Earth Surface Processes and Landforms*, *36*(1), 70–86. https://doi.org/10.1002/esp.2113

Pearson, N. J., & Gingras, M. K. (2006). An ichnological and sedimentological facies model for muddy point-bar deposits. *Journal of Sedimentary Research*, *76*(5), 771–782. https://doi.org/10.2110/jsr.2006.070

Ranasinghe, R., Swinkels, C., Luijendijk, A., Roelvink, D., Bosboom, J., Stive, M., & Walstra, D. (2011). Morphodynamic upscaling with the morfac approach: Dependencies and sensitivities. *Coastal Engineering*, *58*(8), 806–811. https://doi.org/10.1016/j.coastaleng.2011.03.010

Repetto, R., & Tubino, M. (2001). Topographic expressions of bars in channels with variable width. *Physics and Chemistry of the Earth, Part B: Hydrology, Oceans and Atmosphere*, *26*(1), 71–76.

Repetto, R., Tubino, M., & Paola, C. (2002). Planimetric instability of channels with variable width. *Journal of Fluid Mechanics*, *457*, 79–109. https://doi.org/10.1017/S0022112001007595

Rice, S. P., Church, M., Wooldridge, C. L., & Hickin, E. J. (2009). Morphology and evolution of bars in a wandering gravel-bed river: Lower fraser river, British Columbia, Canada. *Sedimentology*, *56*(3), 709–736.

Robinson, A. (1960). Ebb-flood channel systems in sandy bays and estuaries. *Geography*, *45*(3), 183–199.

Roelvink, J. (2006). Coastal morphodynamic evolution techniques. *Coastal Engineering*, *53*(2-3), 277–287. https://doi.org/10.1016/j.coastaleng.2005.10.015

Sambrook Smith, G., Ashworth, P., Best, J., Woodward, J., & Simpson, C. (2006). The sedimentology and alluvial architecture of the sandy braided South Saskatchewan River, Canada. *Sedimentology*, *53*(2), 413–434.

Schramkowski, G., Schuttelaars, H., & De Swart, H. (2002). The effect of geometry and bottom friction on local bed forms in a tidal embayment. *Continental Shelf Research*, *22*(11), 1821–1833. https://doi.org/10.1016/S0278-4343(02)00040-7

Schramkowski, G. P., Schuttelaars, H., & De Swart, H. E. (2004). Non-linear channel–shoal dynamics in long tidal embayments. *Ocean Dynamics*, *54*(3-4), 399–407. https://doi.org/10.1007/s10236-003-0063-6

Schuttelaars, H., & de Swart, H. (2000). Multiple morphodynamic equilibria in tidal embayments. *Journal of Geophysical Research*, *105*(C10), 24,105–24,118. https://doi.org/10.1029/2000JC900110

Schuurman, F., Marra, W. A., & Kleinhans, M. G. (2013). Physics-based modeling of large braided sand-bed rivers: Bar pattern formation, dynamics, and sensitivity. *Journal of geophysical research: Earth Surface*, *118*, 2509–2527. https://doi.org/10.1002/2013JF002896

Seminara, G. (2010). Fluvial sedimentary patterns. *Annual Review of Fluid Mechanics*, *42*, 43–66.

Seminara, G., & Tubino, M. (1989). Alternate bars and meandering free, forced and mixed interactions. In S. Ikeda, & G. Parker (Eds.), *River meandering* (pp. 267–320). Washington, DC: American Geophysical Union.

Seminara, G., & Tubino, M. (2001). Sand bars in tidal channels. Part 1. Free bars. *Journal of Fluid Mechanics*, *440*, 49–74. https://doi.org/10.1017/S0022112001004748

Sistermans, P., & Nieuwenhuis, O. (2004). Western Scheldt estuary (the Netherlands). Amersfoort: DHV group.

Solari, L., Seminara, G., Lanzoni, S., Marani, M., & Rinaldo, A. (2002). Sand bars in tidal channels part 2. Tidal meanders. *Journal of Fluid Mechanics*, *451*, 203–238.

Stefanon, L., Carniello, L., D'Alpaos, A., & Lanzoni, S. (2010). Experimental analysis of tidal network growth and development. *Continental Shelf Research*, *30*(8), 950–962.

Struiksma, N., Olesen, K., Flokstra, C., & De Vriend, H. (1985). Bed deformation in curved alluvial channels. *Journal of Hydraulic Research*, *23*(1), 57–79.

Tambroni, N., Bolla Pittaluga, M., & Seminara, G. (2005). Laboratory observations of the morphodynamic evolution of tidal channels and tidal inlets. *Journal of Geophysical Research*, *110*, F04009. https://doi.org/10.1029/2004JF000243

Tambroni, N., Luchi, R., & Seminara, G. (2017). Can tide dominance be inferred from the point bar pattern of tidal meandering channels? *Journal of Geophysical Research: Earth Surface*, *122*, 492–512. https://doi.org/10.1002/2016JF004139

Tank, F. (1996). Het gedrag van drempels in de westerschelde: Literatuurstudie en hypothesen. IMAU Rapport 96-07, Universiteit Utrecht, Faculteit der Ruimtelijke Wetenschappen, Vakgroep Fysische Geografie.

van Dijk, W., Teske, R., van de Lageweg, W., & Kleinhans, M. (2013). Effects of vegetation distribution on experimental river channel dynamics. *Water Resources Research*, *49*, 7558–7574. https://doi.org/10.1002/2013WR013574

van Dijk, W. M., van de Lageweg, W. I., & Kleinhans, M. G. (2012). Experimental meandering river with chute cutoffs. *Journal of Geophysical Research*, *117*, F03023. https://doi.org/10.1029/2011JF002314

van Veen, J. (1950). Eb-en vloedschaarsystemen in de nederlandse getijwateren. *Tijdschrift Koninklijk Nederlands Aardrijkskundig Genootschap*, *67*, 303–325.

van de Lageweg, W. I., van Dijk, W. M., Baar, A. W., Rutten, J., & Kleinhans, M. G. (2014). Bank pull or bar push: What drives scroll-bar formation in meandering rivers? *Geology*, *42*(4), 319–322.

van der Spek, A. J., & Beets, D. J. (1992). Mid-Holocene evolution of a tidal basin in the western Netherlands: a model for future changes in the northern netherlands under conditions of accelerated sea-level rise? *Sedimentary Geology*, *80*(3), 185–197.

van der Wegen, M., & Roelvink, J. (2008). Long-term morphodynamic evolution of a tidal embayment using a two-dimensional, process-based model. *Journal of Geophysical Research*, *113*, C03016. https://doi.org/10.1029/2006JC003983

Verbeek, H., Wang, Z., & Thoolen, P. (1999). Secondary currents in estuarine morphodynamic modelling: A case-study of the Western Scheldt. River, Coastal and Estuarine Morphodynamics, 649–659.

Visconti, F., Camporeale, C., & Ridolfi, L. (2010). Role of discharge variability on pseudomeandering channel morphodynamics: Results from laboratory experiments. *Journal of Geophysical Research*, *115*, F04042. https://doi.org/10.1029/2010JF001742

Whiting, P. J., & Dietrich, W. E. (1993). Experimental constraints on bar migration through bends: Implications for meander wavelength selection. *Water Resources Research*, *29*(4), 1091–1102. https://doi.org/10.1029/92WR02356

Zhou, Z., Olabarrieta, M., Stefanon, L., D'Alpaos, A., Carniello, L., & Coco, G. (2014). A comparative study of physical and numerical modeling of tidal network ontogeny. *Journal of Geophysical Research: Earth Surface*, *119*, 892–912. https://doi.org/10.1002/2014JF003092

Zolezzi, G., Luchi, R., & Tubino, M. (2012). Modeling morphodynamic processes in meandering rivers with spatial width variations. *Reviews of Geophysics*, *50*, RG4005. https://doi.org/10.1029/2012RG000392